



Breathable and Wearable MXene-Decorated Air-Laid Paper With Superior Folding Endurance and Electromagnetic Interference-Shielding Performances

Chang Ma¹, Tong Liu¹, Wei Xin¹, Guo-Qiang Xi^{1,2} and Ming-Guo Ma^{1*}†

¹ Beijing Key Laboratory of Lignocellulosic Chemistry, Engineering Research Center of Forestry Biomass Materials and Bioenergy, College of Materials Science and Technology, Beijing Forestry University, Beijing, China, ² Key Laboratory for Green Processing of Chemical Engineering of Xinjiang Bingtuan, School of Chemistry and Chemical Engineering, Shihezi University, Shihezi, China

OPEN ACCESS

Edited by:

Jiatao Zhang,
Beijing Institute of Technology, China

Reviewed by:

Jingbo Li,
Beijing Institute of Technology, China
Guozhen Shen,
Institute of Semiconductors
(CAS), China
Xiang Wu,
Shenyang University of
Technology, China

*Correspondence:

Ming-Guo Ma
mg_ma@bjfu.edu.cn

†ORCID:

Ming-Guo Ma
orcid.org/0000-0001-6319-9254

Specialty section:

This article was submitted to
Colloidal Materials and Interfaces,
a section of the journal
Frontiers in Materials

Received: 24 August 2019

Accepted: 14 November 2019

Published: 12 December 2019

Citation:

Ma C, Liu T, Xin W, Xi G-Q and
Ma M-G (2019) Breathable and
Wearable MXene-Decorated Air-Laid
Paper With Superior Folding
Endurance and Electromagnetic
Interference-Shielding Performances.
Front. Mater. 6:308.
doi: 10.3389/fmats.2019.00308

With the development of electronic information technology, electromagnetic shielding pollution has become a thorny environmental problem. Two-dimensional transition metal carbides/nitrides (MXenes) are regarded as the next-generation material for electromagnetic interference (EMI) shielding due to their excellent electrical conductivity and large specific surface area. Flexible membrane-like MXene-based materials in EMI shielding have received tremendous attention, but very few of them can meet the actual needs of durability, stability, and breathability in daily life. In this article, we chose air-laid paper as a flexible substrate for preparing MXene-decorated composite paper by a simple “dipping and drying” method. This composite paper exhibits a high electrical conductivity of 173.0 S m^{-1} , a superior EMI shielding efficiency (more than 90% of the electromagnetic waves in X-band), good mechanical flexibility (more than 9.8×10^4 times), and breathability. Moreover, the composite paper shows excellent durability after folding or soaking in artificial sweat. Therefore, the as-prepared MXene-decorated composite paper has a promising application in EMI-shielding clothing fields.

Keywords: MXene, electromagnetic interference shielding, breathable, wearable, flexible, durable, multi-functional clothing

INTRODUCTION

Along with the development of high technology and the arrival of the electronic age, digital electronic technology has spread to encompass our private lives, our work lives, and our research in every area (Yang et al., 2018; Cao M. et al., 2019; Zhao et al., 2019a). Under such circumstances, the by-product, electromagnetic interference (EMI) pollution, has become a new environment problem (Liu et al., 2019). Therefore, the design and preparation of EMI-shielding materials have become research hotspots (Li and Wang, 2017; Kolanowska et al., 2018). The earliest electromagnetic shielding materials were metals, such as Cu and Ag, and these are expensive, heavy, and non-flexible (Lee et al., 2016; Sankaran et al., 2018). The second-generation EMI-shielding materials are made by electrical conductive carbon, such as a carbon nanotube (CNT) and graphene (Chen et al., 2013; Song et al., 2017; Wan and Li, 2017; Zhao et al., 2019b). It is, however, still difficult for carbon-based EMI-shielding materials to achieve a high EMI-shielding performance at low thicknesses (Weng et al., 2018).

In 2011, Gogosti et al. discovered a series of two-dimensional transition metal carbides/nitrides called MXene, which was produced by selectively etching the A-element from the MAX phase (ternary transition metal carbides/nitrides) (Naguib et al., 2011). After etching, the MXene nanosheets possess abundant surface terminations (OH, O, and F groups), which make it possible to fabricate MXene-based composite materials (Cao M. et al., 2019; Cao W. et al., 2019; Zhou et al., 2019). MXene has been used in the field of EMI shielding owing to its high conductivity and large specific surface area (Sun et al., 2017; Zhang et al., 2018; Bian et al., 2019; Li et al., 2019; Xu et al., 2019). Shahzad et al. reported a kind of MXene film and a MXene-sodium alginate composite film, which exhibited superb EMI-shielding performances of 95 and 25 dB, respectively (Shahzad et al., 2016). Cao et al. (2018) employed the nacre-inspired strategy to design and prepare an MXene/cellulose nanofibers composite film with increase the EMI-shielding performance.

Nevertheless, with the increasing demand for wearable devices today, single-functional materials with high EMI-shielding performances are no longer sufficient (Wang Q. et al., 2019). Although many MXene-based films and textiles were fabricated for flexible EMI shielding, to our knowledge, the flexible MXene membrane-like materials are far from meeting the needs of practical applications. The new generation of EMI-shielding materials should meet wearable, flexible, breathable, and stability requirements. Cellulose paper that is rich in hydroxyl groups may be a potential substrate to fulfill the requirements because of its air permeability, flexibility, disposability, and hydrophilic properties (Lee et al., 2016; Geng et al., 2019). However, ordinary cellulose, in paper such as filter paper or common printing paper, has low mechanical strength and durability.

The air-laid paper used consisted of cellulose and polyester, which has good mechanical properties and folding endurance (Chen et al., 2017; Lin et al., 2018; Ma et al., 2019). The presence of cellulose provided the rich hydroxyl groups for MXene-decoration and the presence of polyester made up for the deficiency of durability of pure cellulose paper. Herein, we have demonstrated a simple “dipping and coating” method for fabricating breathable and wearable MXene-coated air-laid paper with superb folding endurance and EMI-shielding performances. The air-laid paper fibers can be wrapped by the MXene nanosheets driven by Van der Waals forces and hydrogen bonding. The modification of MXene gave the composite papers good conductivity (up to 173.0 S m^{-1}), which further enhanced the EMI-shielding efficiency (more than 90% of the electromagnetic waves in the X-band can be shielded). MXene-coated air-laid paper keeps the breathability, mechanical strength, and flexibility (more than 9.8×10^4 times) of the air-laid paper substrate.

EXPERIMENTAL SECTION

Material

Air-laid paper was purchased from MAXCLEAN Co., and the MAX phase was provided by 11 companies. Lithium fluoride (LiF), hydrochloric acid (HCl), sodium chloride (NaCl), ammonia chloride (NH_4Cl), acetic acid (CH_3COOH), and lactic

acid ($\text{CH}_3\text{CH}(\text{OH})\text{COOH}$) were of analytical grade without further purification and were purchased from Beijing LanYi Chemical Reagents and Consumables Agency, PR China.

Synthesis of MXene

The MXene nanosheets were prepared following the method as reported (Cao et al., 2018). A total of 1 g of MAX phase was stirred for 48 h in a mixture of LiF and HCl at 40°C for etching. Next, the suspension was washed with deionized water during the process of centrifugation. After centrifugation, the obtained suspension was sonicated for 1 h. Then, the supernatant was dispersed of the delaminated $\text{Ti}_3\text{C}_2\text{T}_x$ (MXene) nanosheets.

Preparation of the MXene/Air-Laid Paper Composite Paper

The MXene/air-laid paper composite paper was fabricated via a simple “dipping and drying” method, where the air-laid paper was dipped in the MXene nanosheets dispersion ink and dried at room temperature. A series of samples were named MP-*n* according to the different soaking times (*n* representing the number of soaking times).

Characterization

The morphology of the specimens was characterized through a field-emission scanning electron microscopy (FE-SEM, Hitachi S-4800, Japan) and a transmission electron microscopy (TEM, Hitachi H-800, Japan). Infrared spectroscopy was recorded by a Fourier transform infrared spectrometer (FTIR, Bruker, Germany). X-ray diffraction patterns were recorded on an X-ray diffractometer (XRD, PANalytical, X'Pert Pro MPD, Netherlands). X-ray photoelectron spectroscopy measurements were performed using an X-ray photoelectron spectrometer (XPS, ESCALAB 250Xi, Thermo Scientific, USA). The sheet resistance (R_s) was measured by a four-pin probe resistivity/square resistance tester (ST2258C, Jingge Electronic Technology, PR China) using the standard four-probe method. The mechanical properties were tested by a tensile testing machine (Zwell/Roell, Germany) where the ordinary chuck distance was 10 mm, and the loading rate was 0.2 mm/min. The folding endurance tests were carried out by a paper-folding endurance meter (DCP-MIT 135, Sichuan Changjiang Paper Equipment Co.) under the load of 9.8 N. The EMI shielding properties measurements were performed by a vector network analyzer (PNA-N5244A, Agilent, USA) using the waveguide method within X bands (8.2–12.4 GHz). The total electromagnetic interference shielding effectiveness (SE_T) can be calculated by the following formulas:

$$SE_T = SE_R + SE_A + SE_M \quad (1)$$

$$SE_T = -10 \log(|S_{21}|^2) \quad (2)$$

$$SE_R = -10 \log(1 - |S_{11}|^2) \quad (3)$$

$$SE_A = -10 \log\left(\frac{|S_{21}|^2}{1 - |S_{11}|^2}\right) \quad (4)$$

where S_{11} and S_{21} are scattering parameters, SE_A is the absorption, SE_R is the reflection, and SE_M is the multiple internal

reflections. SE_M can be negligible, if the $SET \geq 15$ dB (Al-Saleh et al., 2013; Kumar et al., 2015).

EMI shielding efficiency (%) is calculated as follow:

$$\text{Shielding efficiency (\%)} = 100 - \left(\frac{1}{10^{\frac{SE}{10}}} \right) \times 100 \quad (5)$$

RESULTS AND DISCUSSION

The preparation of MXene suspension ink and the strategy for the fabrication of MXene-decorated air-laid paper are depicted in **Figure 1**. Before the exfoliation process, the cohesive bulk MAX (Ti_3AlC_2) phase was a dark-gray powder (**Figure 1A**; **Figures S1, S2** in Supplementary Material). After LiF/HCl etching and sonication, the Al layers had been removed selectively (Wang Y. et al., 2019). The obtained delaminated $Ti_3C_2T_x$ ($d-Ti_3C_2T_x$, MXene) nanosheet aqueous suspension was uniform and stable from the Tyndall effect, which was one of the guarantees for fabricating the MXene-decorated air-laid paper (Liu et al., 2017). The morphology of the MXene nanosheets can be seen from the TEM image (**Figure S3** in Supplementary Material), and it can be seen that the well-exfoliated MXene nanosheets were of a flake-like and ultrathin shape (Wang Y. et al., 2019). **Figure S4** in Supplementary Material shows the XRD patterns of the MAX phase and MXene. After exfoliation, the characteristic (002) peak shifted from 9.6° to 7.9° , which was in agreement with the previous report (Lin et al., 2016), further signifying the successful preparation of the MXene nanosheets.

A simple and efficient method called “dipping and drying” has been used in this research, as illustrated in **Figure 1B**. The fabrication process of composite papers included dipping air-laid papers in MXene suspension ink and repeating the dipping and drying processes for the deposition of MXene nanosheets on the air-laid paper fibers. Air-laid paper consists of cellulose and polyester without any binders or additives. Cellulose is hydrophilic due to the presence of hydroxyl groups. Therefore, air-laid papers without any pretreatment can be covered by the MXene driven by van der Waals forces and hydrogen bonding between MXene nanosheets and cellulose in the “dipping and drying” process. In addition, the presence of polyester fiber can make up for the shortcomings of the poor durability of cellulose. After being MXene decorated, the composite papers are then endowed with good electrical conductivity. In this article, a series of tests have been conducted on the structure, performance, and stability of composite papers. It was expected that the obtained composite papers would have an opportunity to be applied in the preparation of breathable clothing with good EMI-shielding performance.

In order to explore the composite paper further, a series of tests were performed. The characterization results of FTIR, XRD, and XPS are illustrated in **Figure 2**. The FTIR spectra of the original air-laid paper, pure MXene, and obtained composite paper are shown in **Figure 2A**. Two typical peaks of C-F ($1,390\text{ cm}^{-1}$) and C-OH (584 cm^{-1}) were observed in the FTIR spectrum of pure MXene. After soaking in the MXene suspension ink, the composite paper still had the representative

characteristic bands of cellulose, including $3,450\text{ cm}^{-1}$ (-OH stretching vibration), $2,920\text{ cm}^{-1}$ (C-H stretching vibration), $1,700\text{ cm}^{-1}$ (-OH bending vibration), and $1,100\text{ cm}^{-1}$ (C-O stretching vibration) (Cao et al., 2018). The XRD patterns of the pure MXene, original air-laid paper, and composite paper are shown in **Figure 2B**. The peaks at $2\theta = 14.7\text{--}17.2^\circ$ of the original air-laid paper and composite paper correspond to (101) and (101) crystal planes of cellulose I, and the diffraction band at $2\theta = 22.8^\circ$ corresponds to the (002) crystal plane of cellulose I (Cui et al., 2019). The peak at $2\theta = 25.8^\circ$ represents the (100) crystal plane of polyester crystalline structure (Phang et al., 2004). What is more, after being MXene-decorated, the characteristic (002) peak of MXene shifted from $2\theta = 7.9$ to 6.3° , indicating that the d-spacing of MXene nanosheets increased (Cao et al., 2018). The XPS spectra are shown in **Figure 2C**. It is obvious that the composite paper included the peak of Ti element, which comes from the MXene nanosheets. All the above experimental results show that the MXene nanosheets have been successfully introduced into the composite papers as prepared.

Figures 3A–G compare the microstructure and surface morphology of the original air-laid paper and the composite papers in different “dipping and drying” cycles. It was clear that the fabric structure can be well-maintained, and the space among the fibers were not clogged after “dipping and drying” process (**Figures 3A,B**), which is beneficial to keep the breathability of air-laid paper (the gas permeability test will be mentioned in **Figure 5J**). The composite papers showed rougher fiber surfaces coated with a pleated MXene layer, compared with the smooth surfaces of original air-laid paper fibers, and the roughness was increased with the dipping–drying cycles (**Figures 3C–G**). All fiber surfaces were almost covered with MXene sheets after 30 cycles (**Figure 3G**). As shown in **Figure 3H**, the energy-dispersive X-ray spectroscopy (EDS) elemental map confirmed the uniform distribution of the MXene layer on the fiber surface.

In order to display the appearance and characteristics more intuitively, the digital photos of composite papers were shown in **Figures 3I–M**. With the increase in soaking times, the color of composite papers became deeper, finally becoming black (**Figure 3I**). **Figure 3J** is a photographic image of a white and a black paper crane folded by original air-laid paper and MP-10, exhibiting that the original air-laid paper or MP composite paper is highly flexible and foldable. Not only could it be folded, but the composite papers can also be cut into different shapes, such as star or heart, as shown in **Figure 3K**. The composite papers are light enough to be placed on a leaf without crushing this leaf (**Figure 3L**). Furthermore, the sizes and shapes of the composite papers depend on the air-laid paper substrate so that composite papers of any shapes and sizes can be prepared (**Figure 3M**).

Electrical conductivity is one of the factors affecting the level of EMI shielding efficiency (Liu et al., 2017). As shown in **Figure 4A**, with the increasing of dip-coating cycles, the conductivity of composite paper increases rapidly. When the cycle reaches 20 times, high electrical conductivity is up to 173.0 S m^{-1} . The brightness of a small bulb can also intuitively explain

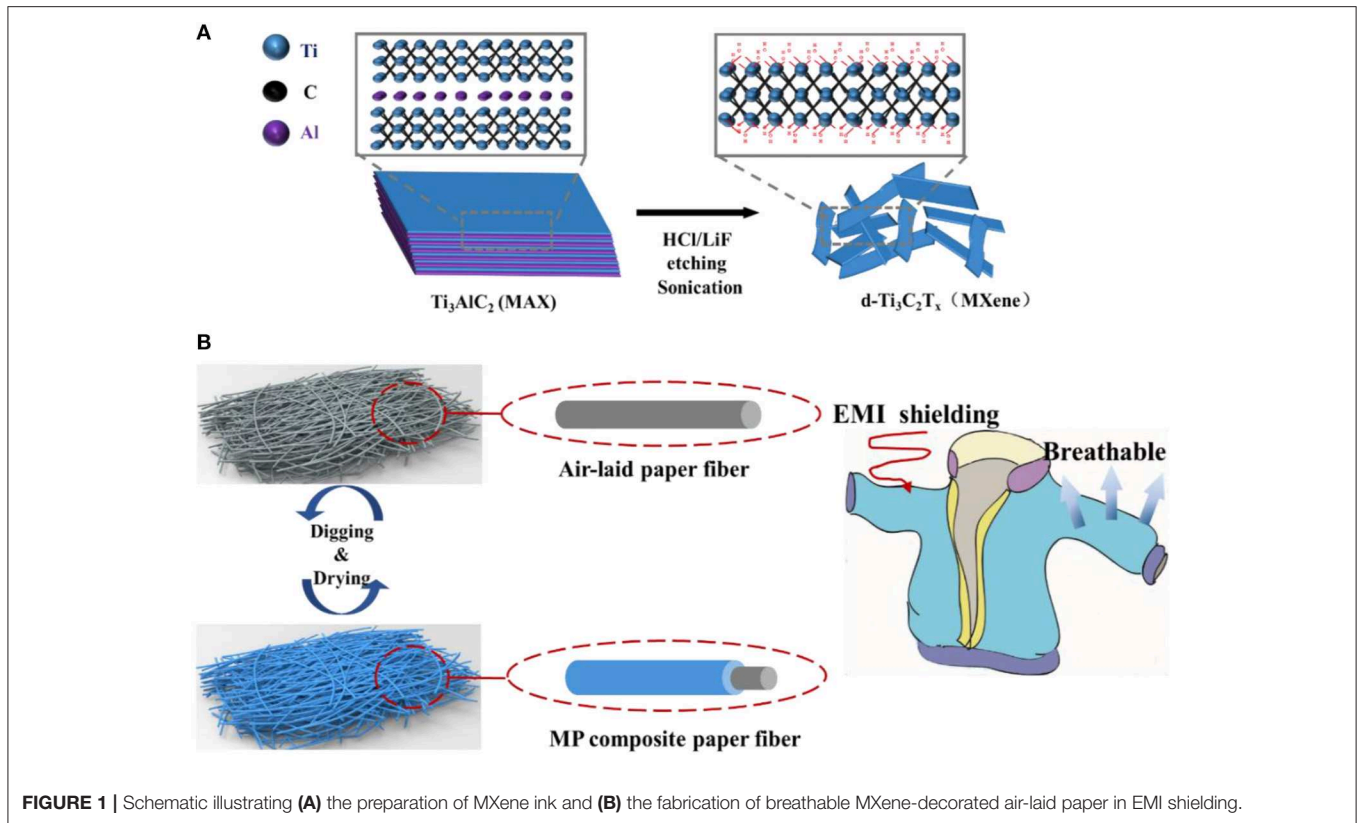


FIGURE 1 | Schematic illustrating (A) the preparation of MXene ink and (B) the fabrication of breathable MXene-decorated air-laid paper in EMI shielding.

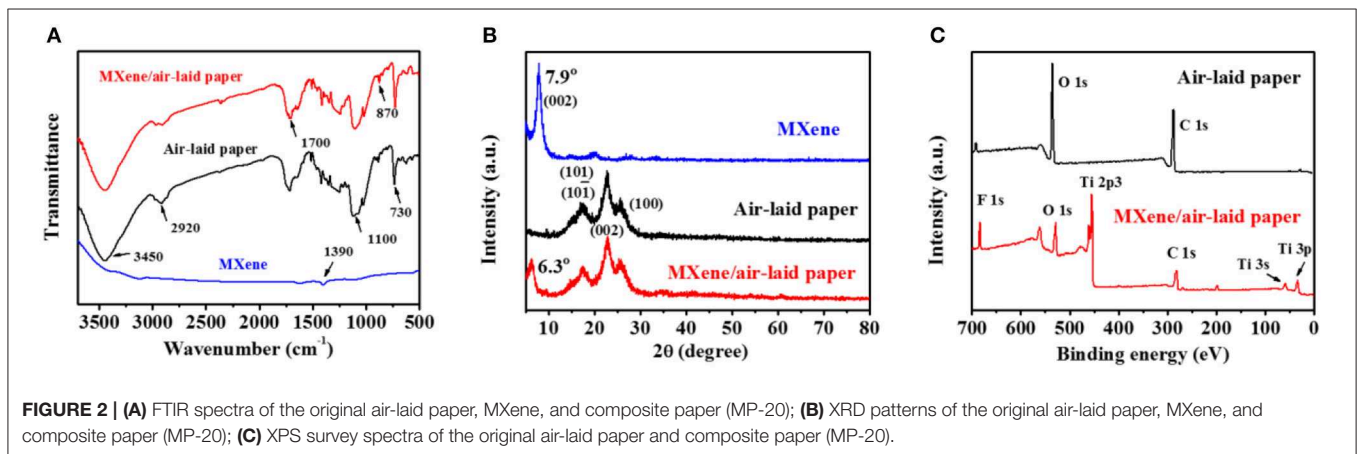
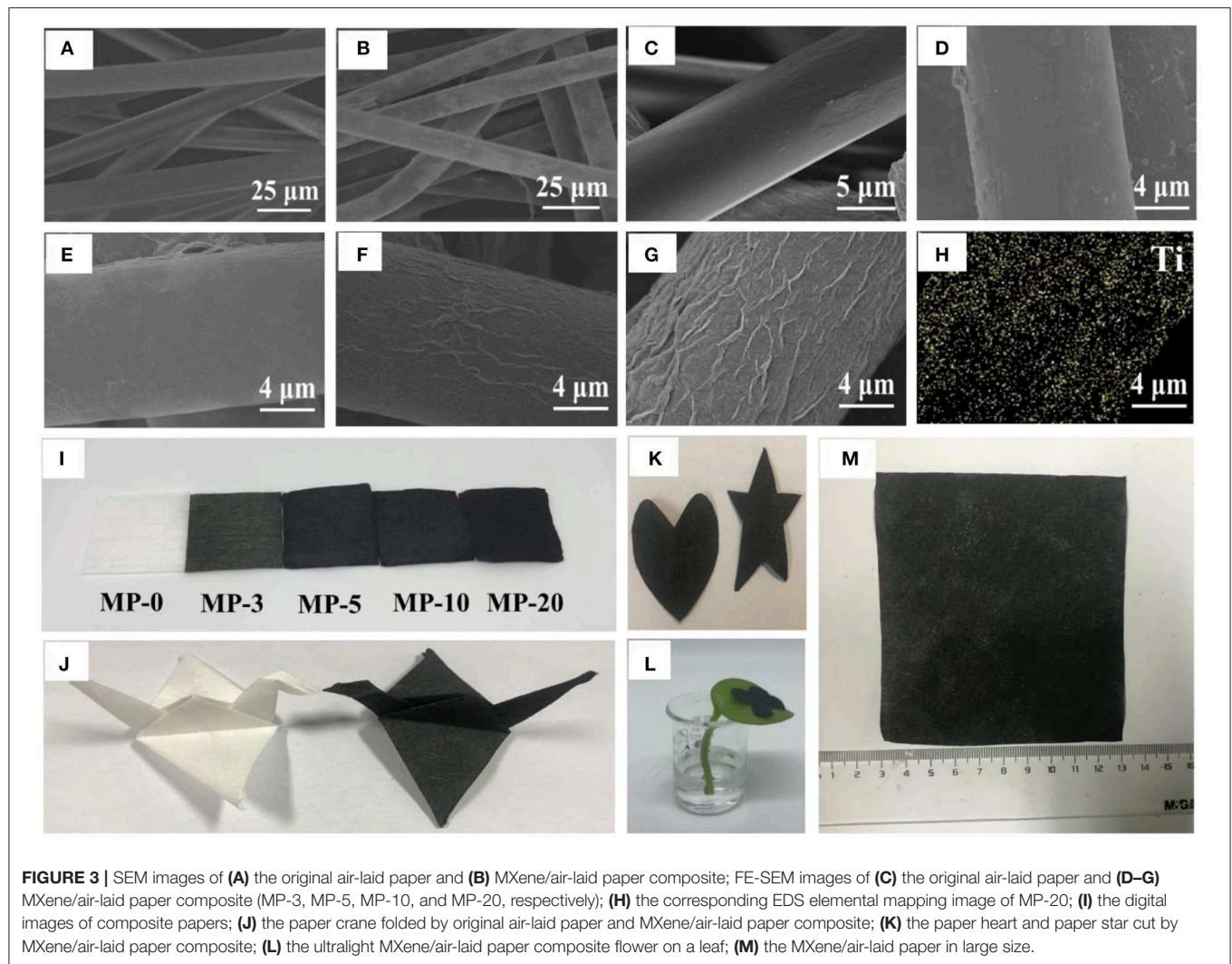


FIGURE 2 | (A) FTIR spectra of the original air-laid paper, MXene, and composite paper (MP-20); (B) XRD patterns of the original air-laid paper, MXene, and composite paper (MP-20); (C) XPS survey spectra of the original air-laid paper and composite paper (MP-20).

the results of the electrical conductivity, which were described above. The reason for these results may be the increase in mass loading. **Figure 4B** illustrates the plots of thickness and mass loading vs. dipping times for composite papers in different dipping times. Unlike mass loading, the changes in thickness are not very obvious. This may be because the MXene nanosheets mainly covered the single fiber surfaces rather than the entire surfaces of air-laid papers.

The obtained composite papers exhibited outstanding EMI-shielding performances (**Figure 4C**). The composite papers in different “dipping and drying” cycles exhibited an EMI-shielding

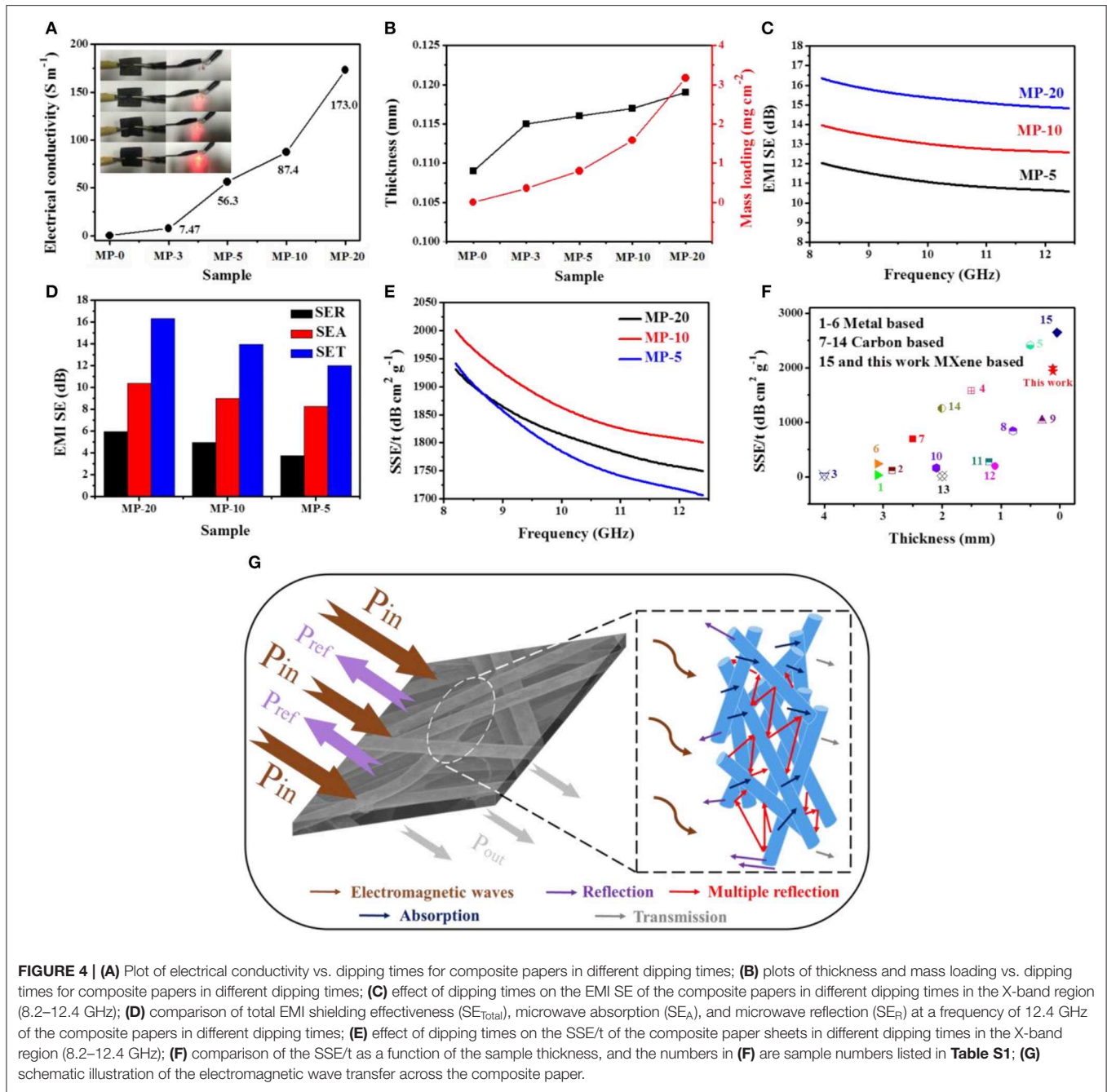
effectiveness of >10 dB over the whole X-band, illustrating that composite papers can shield more than 90% of the electromagnetic waves in the X-band effectively, according to the formula (5). The EMI-shielding efficiency increases with the increase in dipping cycles, which is similar to the variation trend of electrical conductivity. When the cycle reaches 20 times, an EMI shielding efficiency is up to 16.36 dB. To learn more about EMI-shielding mechanisms of composite papers, the comparisons of microwave absorption (SE_A) and microwave reflection (SE_R) to the total EMI shielding effectiveness (SE_T) were investigated, as seen in **Figure 4D**. It should be clear that



the absorption part is always larger than the reflection part for all the samples. For example, the SE_T , SE_A , and SE_R of the MP-20 were ~ 16.36 , 10.41 , and 5.95 dB at a frequency of 8.2 GHz. These results indicated that the EMI-shielding effectiveness of composite papers was absorption oriented. To show the practicality of the specimen better, the thickness and weight of samples should be taken into account. A specific SE value of SSE/t (SE divided by the density and thickness of the specimen) is therefore more widely used to evaluate the EMI-shielding effectiveness. **Figure 4E** shows that the SSE/t values of composite papers were all more than $1,700$ dB cm^2 g^{-1} , and among them, the SSE/t values of MP-10 reached $2,000.92$ dB cm^2 g^{-1} . As shown in **Figure 4F** and **Table S1** in Supplementary Material, the composite papers with ultrathin thickness and ultralight weight exhibited a better EMI-shielding performance compared with metal-based and carbon-based shielding materials. Based on all the above results, the EMI-shielding mechanism of composite papers is illustrated in **Figure 4G**, among which there are three kinds of possible attenuation mechanisms. When an incident electromagnetic wave radiates to the composite paper, part of

the electromagnetic wave is reflected while the rest interacts with the conductive MXene, which results in energy dissipation of electromagnetic waves. In addition, the multiple internal reflections between composite paper fibers also contributes to the loss of electromagnetic energy (Wang Q. et al., 2019).

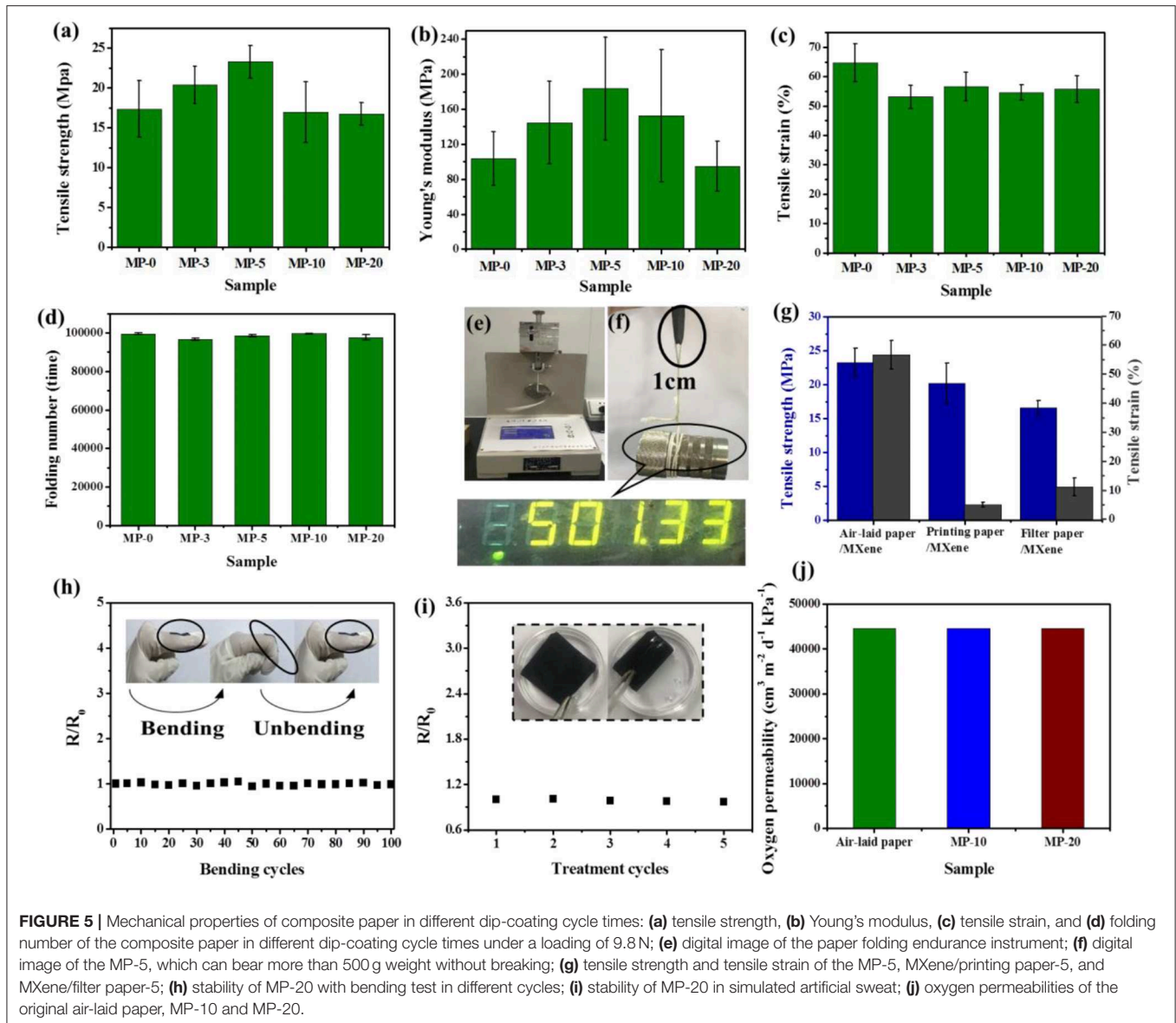
The mechanical properties of original air-laid paper and composite papers were tested, as shown in **Figure 5**, and the detailed values are listed in **Table S2**. The results suggested that composite papers exhibited excellent strength and folding endurance behaviors. The original air-laid paper showed a tensile strength of 17.34 ± 3.55 MPa, a fracture strain of $64.72 \pm 6.49\%$, and Young's modulus of 103.7 ± 30.49 MPa. With the increasing of dipping times from 3 to 20, the tensile strength of the composite paper increases from 20.36 ± 2.34 to 23.26 ± 2.07 MPa then decreased to 16.73 ± 1.45 MPa (**Figure 5a**), the Young's modulus increased from 144.69 ± 47.41 to 183.57 ± 58.84 MPa and then decreased to 94.7 ± 28.73 MPa (**Figure 5b**). As shown in **Figure 5f**, the MP-5 composite paper with a width of 10 mm can bear more than 500 g weight without breaking. While the tensile strain of composite papers is slightly lower than



that of original air-laid paper, however, all the tensile strain of the composite paper was bigger than 50% (Figure 5c). Especially worth mentioning was the superior folding endurance of the composite papers, which were measured by a paper-folding endurance instrument under a 9.8 N pulling load, as given in Figure 5e. All the composite papers could be folded for more than 9.8×10^4 times, proving that the dipping and drying process had no significant effect on folding endurance (Figure 5d). As far as we know, the existing studies of flexible MXene membrane-like materials have either failed to measure the folding endurance accurately or obtained very low values, and they have therefore

come far from meeting the needs of practical applications. To further demonstrate the superiority of the composite papers, the samples fabricated by other cellulose-based substrates with similar preparation methods and conditions were also tested. As can be seen from Figure 5g, the MP-5 shows prominent advantages in tensile stress and elongation capacity, compared with those of MXene/printing paper-5 and MXene/filter paper-5, because the polyester can make up for the lack of cellulose in mechanical performance.

Not only that, but the composite papers also have stable conductivity and good durability. As shown in Figure 5h, the



sheet resistance variations of MP-20 under different cycles have been tested, and no conspicuous increase or decrease during the test. The sheet resistance variations of MP-20 in simulated artificial sweat had also been measured. The simulated artificial sweat solution was prepared according to the previous reports (20 g L^{-1} NaCl, 17.5 g L^{-1} NH_4Cl , 5 g L^{-1} acetic acid, and 15 g L^{-1} lactic acid; pH 4.7) (Park et al., 2018). After five times of soaking in the simulated artificial sweat, there were no significant changes in the sheet resistance of MP-20. The test results proved that the composite papers exhibited performance stability to satisfy the application in different conditions in real life. What is more, the oxidation stability of the MXene-decorated air-laid paper has also been concerned. As shown in Figure S5, there were no significant changes in the visual appearance and resistance, so that the MP-20 achieved outstanding long-term oxidation stability over 5 weeks in the

air at room temperature. For further confirming the folding endurance and durability of the as-prepared product, the SEM images are shown in Figure S6. There were no obvious changes between Figure S6A and Figures S6B–D, which is direct proof of the folding endurance and durability of MXene-decorated air-laid paper. For further exploring the practicality of composite paper, the gas (oxygen) permeability of the original air-laid paper and the MXene-decorated air-laid papers (MP-10 and MP-20) have been tested. It is obvious that the dipping and drying process did not have an effect on the gas permeability of composite papers. This is confirmed in the SEM images (Figures 3A,B): The fabric structure can be well-maintained, and the space among the fibers is not clogged after “dipping and drying” process.

Based on the above-mentioned results, MXene-decorated air-laid composite paper exhibited outstanding flexibility, durability,

stable conductivity, and breathability, indicating that it has great promising potential to be applied in EMI-shielding clothing in our daily life.

CONCLUSION

In conclusion, we demonstrated a kind of flexible, breathable, wearable, and stable MXene-decorated air-laid paper with superb folding endurance and the EMI-shielding performance by a simple “dipping and drying” method. The air-laid papers can be covered by the MXene driven by van der Waals forces and hydrogen bonding between MXene nanosheets and cellulose in “dipping and drying” process. In addition, the presence of polyester fiber can make up for the shortcomings of poor durability of cellulose. The composite paper exhibited a high electrical conductivity of 173.0 S m^{-1} , a superior EMI-shielding efficiency (more than 90% of the electromagnetic waves in X-band can be shielded), good mechanical flexibility (more than 9.8×10^4 times can be folded), and breathability. Moreover, the composite papers showed excellent durability after folding and treating by artificial sweat. Thus, the prepared composite paper had the advantages of superior EMI-shielding performance, flexibility, durability, stable conductivity, and breathability. It is expected that this material will have promising potential to be applied in EMI-shielding clothing fields.

REFERENCES

- Al-Saleh, M. H., Saadeh, W. H., and Sundararaj, U. (2013). EMI shielding effectiveness of carbon based nanostructured polymeric materials: a comparative study. *Carbon* 60, 146–156. doi: 10.1016/j.carbon.2013.04.008
- Bian, R., He, G., Zhi, W., Xiang, S., Wang, T., and Cai, D. (2019). Ultralight MXene-based aerogels with high electromagnetic interference shielding performance. *J. Mater. Chem. C* 7, 474–478. doi: 10.1039/C8TC04795B
- Cao, M., Cai, Y., He, P., Shu, J., Cao, W., and Yuan, J. (2019). 2D MXenes: electromagnetic property for microwave absorption and electromagnetic interference shielding. *Chem. Eng. J.* 359, 1265–1302. doi: 10.1016/j.cej.2018.11.051
- Cao, W., Chen, F., Zhu, Y., Zhang, Y., Jiang, Y., Ma, M., et al. (2018). Binary strengthening and toughening of MXene/cellulose nanofiber composite paper with nacre-inspired structure and superior electromagnetic interference shielding properties. *ACS Nano* 12, 4583–4593. doi: 10.1021/acsnano.8b00997
- Cao, W., Feng, W., Jiang, Y., Ma, C., Zhou, Z., Ma, M., et al. (2019). Two-dimensional MXene-reinforced robust surface superhydrophobicity with self-cleaning and photothermal-actuating binary effects. *Mater Horizons* 6, 1057–1065. doi: 10.1039/C8MH01566J
- Chen, Y., Cai, K., Liu, C., Song, H., and Yang, X. (2017). High-performance and breathable polypyrrole coated air-laid paper for flexible all-solid-state supercapacitors. *Adv. Energy Mater.* 7:1701247. doi: 10.1002/aenm.201701247
- Chen, Z., Xu, C., Ma, C., Ren, W., and Cheng, H. (2013). Lightweight and flexible graphene foam composites for high-performance electromagnetic interference shielding. *Adv. Mater.* 25, 1296–1300. doi: 10.1002/adma.201204196
- Cui, C., Xiang, C., Geng, L., Lai, X., Guo, R., Zhang, Y., et al. (2019). Flexible and ultrathin electrospun regenerate cellulose nanofibers and d-Ti3C2Tx (MXene) composite film for electromagnetic interference shielding. *J. Alloys Comp.* 788, 1246–1255. doi: 10.1016/j.jallcom.2019.02.294

DATA AVAILABILITY STATEMENT

The raw data supporting the conclusions of this manuscript will be made available by the authors, without undue reservation, to any qualified researcher.

AUTHOR CONTRIBUTIONS

M-GM and CM conceived and designed the experiments. CM performed the experiments. TL, WX, and G-QX contributed reagents, materials, and analysis tools. CM, TL, WX, G-QX, and M-GM analyzed the data and wrote the paper.

FUNDING

The financial support received from the Beijing Forestry University Outstanding Young Talent Cultivation Project (2019JQ03014) and the Key Production Innovative Development Plan of the Southern Bingtuan (2019DB007) is gratefully acknowledged.

SUPPLEMENTARY MATERIAL

The Supplementary Material for this article can be found online at: <https://www.frontiersin.org/articles/10.3389/fmats.2019.00308/full#supplementary-material>

- Geng, L., Zhu, P., Wei, Y., Guo, R., Xiang, C., Cui, C., et al. (2019). A facile approach for coating Ti3C2Tx on cotton fabric for electromagnetic wave shielding. *Cellulose* 26, 2833–2847. doi: 10.1007/s10570-019-02284-5
- Kolanowska, A., Janas, D., Herman, A. P., Jedrysiak, R. G., Gizewski, T., and Boncel, S. (2018). From blackness to invisibility – carbon nanotubes role in the attenuation of and shielding from radio waves for stealth technology. *Carbon* 126, 31–52. doi: 10.1016/j.carbon.2017.09.078
- Kumar, P., Shahzad, F., Yu, S., Hong, S. M., Kim, Y., and Koo, C. M. (2015). Large-area reduced graphene oxide thin film with excellent thermal conductivity and electromagnetic interference shielding effectiveness. *Carbon* 94, 494–500. doi: 10.1016/j.carbon.2015.07.032
- Lee, T., Lee, S., and Jeong, Y. G. (2016). Highly effective electromagnetic interference shielding materials based on silver nanowire/cellulose papers. *ACS Appl. Mater. Interfaces* 8, 13123–13132. doi: 10.1021/acsmi.6b02218
- Li, X., Yin, X., Liang, S., Li, M., Cheng, L., and Zhang, L. (2019). 2D carbide MXene Ti2CTX as a novel high-performance electromagnetic interference shielding material. *Carbon* 146, 210–217. doi: 10.1016/j.carbon.2019.02.003
- Li, Z. B., and Wang, Y. G. (2017). Preparation of polymer-derived graphene-like carbon-silicon carbide nanocomposites as electromagnetic interference shielding material for high temperature applications. *J. Alloys Comp.* 709, 313–321. doi: 10.1016/j.jallcom.2017.03.080
- Lin, H., Wang, X., Yu, L., Chen, Y., and Shi, J. (2016). Two-dimensional ultrathin MXene ceramic nanosheets for photothermal conversion. *Nano Lett.* 17, 384–391. doi: 10.1021/acs.nanolett.6b04339
- Lin, X., Yang, M., Hong, W., Yu, D., and Chen, X. (2018). Commercial fiber products derived free-standing porous carbonized-membranes for highly efficient solar steam generation. *Front. Mater.* 5:74. doi: 10.3389/fmats.2018.00074
- Liu, H., Zhao, D., Liu, Y., Hu, P., Wu, X., and Xia, H. (2019). Boosting energy storage and electrocatalytic performances by synergizing CoMoO4@MoZn22 core-shell structures. *Chem. Eng. J.* 373, 485–492. doi: 10.1016/j.cej.2019.05.066

- Liu, J., Zhang, H., Sun, R., Liu, Y., Liu, Z., Zhou, A., et al. (2017). Hydrophobic, flexible, and lightweight mxene foams for high-performance electromagnetic-interference shielding. *Adv. Mater.* 29:1702367. doi: 10.1002/adma.201702367
- Ma, C., Cao, W., Xin, W., Bian, J., and Ma, M. (2019). Flexible and free-standing reduced graphene oxide and polypyrrole coated air-laid paper-based supercapacitor electrodes. *Ind. Eng. Chem. Res.* 58, 12018–12027. doi: 10.1021/acs.iecr.9b02088
- Naguib, M., Kurtoglu, M., Presser, V., Lu, J., Niu, J., Heon, M., et al. (2011). Two-dimensional nanocrystals produced by exfoliation of Ti₃AlC₂. *Adv. Mater.* 23, 4248–4253. doi: 10.1002/adma.201102306
- Park, S. W., Han, G. D., Choi, H. J., Prinz, F. B., and Shim, J. H. (2018). Evaluation of atomic layer deposited alumina as a protective layer for domestic silver articles: anti-corrosion test in artificial sweat. *Appl. Surf. Sci.* 441, 718–723. doi: 10.1016/j.apsusc.2018.02.090
- Phang, I. Y., Pramoda, K. P., Liu, T., and He, C. (2004). Crystallization and melting behavior of polyester/clay nanocomposites. *Polymer Int.* 53, 1282–1289. doi: 10.1002/pi.1513
- Sankaran, S., Deshmukh, K., Ahamed, M. B., and Khadheer Pasha, S. K. (2018). Recent advances in electromagnetic interference shielding properties of metal and carbon filler reinforced flexible polymer composites: a review. *Compos. A Appl. Sci. Manuf.* 114, 49–71. doi: 10.1016/j.compositesa.2018.08.006
- Shahzad, F., Alhabeb, M., Hatter, C. B., Anasori, B., Hong, S. M., Koo, C. M., et al. (2016). Electromagnetic interference shielding with 2D transition metal carbides (MXenes). *Science* 350, 1137–1140. doi: 10.1126/science.aag2421
- Song, Q., Ye, F., Yin, X., Li, W., Li, H., Liu, Y., et al. (2017). Carbon nanotube-multilayered graphene edge plane core-shell hybrid foams for ultrahigh-performance electromagnetic-interference shielding. *Adv. Mater.* 29:1701583. doi: 10.1002/adma.201701583
- Sun, R., Zhang, H., Liu, J., Xie, X., Yang, R., Li, Y., et al. (2017). Highly conductive transition metal carbide/carbonitride(mxene)/polystyrene nanocomposites fabricated by electrostatic assembly for highly efficient electromagnetic interference shielding. *Adv. Func. Mater.* 27:1702807. doi: 10.1002/adfm.201702807
- Wan, C., and Li, J. (2017). Synthesis and electromagnetic interference shielding of cellulose-derived carbon aerogels functionalized with α -Fe₂O₃ and polypyrrole. *Carbohydr. Polymers* 161, 158–165. doi: 10.1016/j.carbpol.2017.01.003
- Wang, Q., Zhang, H., Liu, J., Zhao, S., Xie, X., Liu, L., et al. (2019). Multifunctional and water-resistant MXene-decorated polyester textiles with outstanding electromagnetic interference shielding and Joule heating performances. *Adv. Func. Mater.* 29:1806819. doi: 10.1002/adfm.201806819
- Wang, Y., Wang, X., Li, X., Bai, Y., Xiao, H., Liu, Y., et al. (2019). Engineering 3D ion transport channels for flexible mxene films with superior capacitive performance. *Adv. Func. Mater.* 29:1900326. doi: 10.1002/adfm.201900326
- Weng, G., Li, J., Alhabeb, M., Karpovich, C., Wang, H., Lipton, J., et al. (2018). Layer-by-layer assembly of cross-functional semi-transparent MXene-carbon nanotubes composite films for next-generation electromagnetic interference shielding. *Adv. Func. Mater.* 28:1803360. doi: 10.1002/adfm.201803360
- Xu, H., Yin, X., Li, X., Li, M., Liang, S., Zhang, L., et al. (2019). Lightweight Ti₂CTx MXene/Poly(vinyl alcohol) composite foams for electromagnetic wave shielding with absorption-dominated feature. *ACS Appl. Mater. Interfaces* 11, 10198–10207. doi: 10.1021/acsami.8b21671
- Yang, W., Shao, B., Liu, T., Zhang, Y., Huang, R., Chen, F., et al. (2018). Robust and mechanically and electrically self-healing hydrogel for efficient electromagnetic interference shielding. *ACS Appl. Mater. Interfaces* 10, 8245–8257. doi: 10.1021/acsami.7b18700
- Zhang, X., Zhang, Z., and Zhou, Z. (2018). MXene-based materials for electrochemical energy storage. *J. Energy Chem.* 27, 73–85. doi: 10.1016/j.jechem.2017.08.004
- Zhao, D., Dai, M., Liu, H., Xiao, L., Wu, X., and Xia, H. (2019a). Constructing high performance hybrid battery and electrocatalyst by heterostructured NiCo₂O₄@NiWS nanosheets. *Crys. Growth Design* 19, 1921–1929. doi: 10.1021/acs.cgd.8b01904
- Zhao, D., Liu, H., and Wu, X. (2019b). Bi-interface induced multi-active MCo₂O₄@MCo₂S₄@PPy (M=Ni, Zn) sandwich structure for energy storage and electrocatalysis. *Nano Energy* 57, 363–370. doi: 10.1016/j.nanoen.2018.12.066
- Zhou, Z., Liu, J., Zhang, X., Tian, D., Zhan, Z., and Lu, C. (2019). Ultrathin MXene/calcium alginate aerogel film for high-performance electromagnetic interference shielding. *Adv. Mater. Interfaces* 6:1802040. doi: 10.1002/admi.201802040

Conflict of Interest: The authors declare that the research was conducted in the absence of any commercial or financial relationships that could be construed as a potential conflict of interest.

Copyright © 2019 Ma, Liu, Xin, Xi and Ma. This is an open-access article distributed under the terms of the Creative Commons Attribution License (CC BY). The use, distribution or reproduction in other forums is permitted, provided the original author(s) and the copyright owner(s) are credited and that the original publication in this journal is cited, in accordance with accepted academic practice. No use, distribution or reproduction is permitted which does not comply with these terms.